Supporting Online Materials (SOM) for:

Spiroindolones, potent chemotype for the treatment of malaria

Matthias Rottmann, Case McNamara, Bryan K. S. Yeung, Marcus C.S. Lee, Bin Zou, Bruce Russell, Patrick Seitz, David M. Plouffe, Neekesh V. Dharia, Jocelyn Tan, Steven B. Cohen, Kathryn R. Spencer, Gonzalo E. González-Páez, Suresh B. Lakshminarayana, Anne Goh, Rossarin Suwanarusk, Timothy Jegla, Esther K. Schmitt, Hans-Peter Beck, Reto Brun, Francois Nosten, Laurent Renia, Veronique Dartois, Thomas H. Keller, David A. Fidock, Elizabeth A. Winzeler, and Thierry T. Diagana

This supplement contains:

Table of Contents

Supplemental Tables

Table S1. *In vitro* antimalarial activity of NITD609 against various culture-adapted *Plasmodium falciparum* strains

P. falciparum strains	Resistance	IC_{50} (nM)[1]
NF54		0.5 ± 0.1
3D7		0.7 ± 0.2
K1	Chloroquine, Pyrimethamine	0.6 ± 0.2
W2	Chloroquine, Pyrimethamine	0.9 ± 0.1
7G8	Pyrimethamine	1.2 ± 0.5
TM90C2A	Chloroquine, Mefloquine, Pyrimethamine	0.5 ± 0.1
TM91C235	Chloroquine, Mefloquine, Pyrimethamine	0.9 ± 0.1
D6		1.0 ± 0.2
V1/S	Chloroquine, Pyrimethamine	1.4 ± 0.2

[1] IC_{50} values expressed as mean±SD of at least three independent assays

Table S2. NITD609 *in vitro* cytotoxicity assessment

Cell Line	C6 Glioma	THP1	HepG2	BHK21
CC_{50} (µM)	>50	14 ± 0.4	>25	>25

Table S3. NITD609 hERG binding and patch clamp assay data

Assay	Inhibition (%)[1]	IC_{50} (µM)
Binding	52	30.44
Patch clamp	44.9	> 30.0

[1] Inhibition measured at 30 µM NITD609

Table S4. NITD609 binding to recombinant receptors

In vitro recombinant protein binding assay	Species	IC_{50} (µM)	*In vitro* recombinant protein binding assay	Species	IC_{50} (µM)
Adenosine 2A receptor	Human	>30	Glucagon receptor	Human	>30
Adenosine 3 receptor	Human	8.3	Glucocorticoid receptor	Human	>30
Adenosine transporter	Human	>30	Ghrelin receptor	Human	>30
Adrenergic Beta 1	Human	>10	Histamine H1 receptor	Human	>10
Adrenergic Beta 2	Human	>10	Histamine H2 receptor	Human	>10
Adrenergic Beta 3	Human	>30	Histamine H3 receptor	Human	>10
Alpha 1A receptor	Human	>10	Melanocortin MC3 receptor	Human	>30
Alpha 2A receptor	Human	>10	Melanocortin MC4 receptor	Human	>30
Alpha 2B receptor	Human	>10	Monoamine Oxydase A	Human	>10
Alpha 2C receptor	Human	>10	Motilin receptor	Human	>10
Androgen receptor	Human	>30	Muscarinic M1 receptor	Human	>10
Angiotensin II AT1 receptor	Human	>30	Muscarinic M2 receptor	Human	>10
Benzodiazepine receptor	Rat	>10	Muscarinic M3 receptor	Human	>10
Bradykinin 1 receptor	Human	>30	Neurokinin NK1 receptor	Human	>10
Bradykinin 2 receptor	Human	>30	NeuropeptideY Y1 receptor	Human	>10
Calcium Channel (L) recept.	Rat	>10	NeuropeptideY Y2 receptor	Human	>10
Calcium Channel (N) recept.	Rat	>10	Neurotensin NT1 receptor	Human	>10
Cannabinoid 1 receptor	Human	>10	Niacin Receptor	Human	>10
Cholecystokinin A receptor	Human	>30	Nicotinic (CNS) receptor	Human	>10
Cholecystokinin B receptor	Human	>30	NMDA channel site recpt.	Human	>10
COX-1 assay	Human	>30	Norepinephrine Transporter	Human	>10
COX-2 assay	Human	>30	Opiate Delta receptor	Human	>10
CRF1 receptor	Human	>30	Opiate Kappa receptor	Human	>10
CRF2alpha receptor	Human	>30	Opiate Mu receptor	Human	>10
Dopamine D1 receptor	Human	>10	Phosphodiesterase 3	Human	>10
Dopamine D2 receptor	Human	>10	Phosphodiesterase 4D	Human	>10
Dopamine D3 receptor	Human	>10	Serotonin 5-HT 1 A recept.	Human	>10
Dopamine D4.4 receptor	Human	>10	Serotonin 5-HT 2A receptor	Human	>10
Dopamine Transporter	Human	>10	Serotonin 5-HT 2B receptor	Human	>10
Endothelin A receptor	Human	>30	Serotonin 5-HT 2C receptor	Human	>10
Endothelin B receptor	Human	>30	Serotonin 5-HT3 receptor	Human	>10
Estrogen alpha receptor	Human	>30	Serotonin Transporter	Human	>10
Estrogen beta receptor	Human	>30	Thromboxane A2 receptor	Human	>30
GABA A receptor	Human	>10	Vasopressin V1a receptor	Human	>10
GIP receptor	Rat	>30	Vasopressin V2 receptor	Human	>30

Table S5. Pharmacokinetic parameters of NITD609 in female CD-1 mice and Wistar rats following intravenous (i.v.) and oral (p.o.) administration

Species	Actual dose (mg/kg)	Route	C_{max} (μM)	T_{max} (h)	AUC_{inf} (μM*h)	F (%)	V_{ss} (L/kg)	CL (mL/min/kg)	Elim. $T_{1/2}$(hour)
Mice	5.4	i.v.	—	—	23.88	—	2.11	9.75	3.44
	24.6	p.o.	9.17	1	138.65	100	—	—	10.02
Rats	5	i.v.	—	—	61.32	—	3.04	3.48	10.69
	23.7	p.o.	11.68	8	524.15	100	—	—	27.73

Table S6. NITD609 *in vitro* metabolic clearance in liver microsome preparations

Species	Mouse	Rat	Dog	Monkey	Human
CL_h (mL/min/kg)	49.74	5.80	22.07	6.05	8.67

Measured as described in Lau et al. 2002 (S*1*). Intrinsic clearance of NITD609 is predicted to be low in mice, rats, monkeys and humans.

Table S7. Effective doses in an experimental malaria mouse model[1]

compound	ED_{50} (mg/kg)	ED_{90} (mg/kg)	ED_{99} (mg/kg)
NITD609[2]	1.2	2.7	5.3
Artesunate[3]	6.2	32	135
Mefloquine[3]	4.2	6.2	8.6
Chloroquine[3]	1.9	4.2	8.4

[1] Effective doses resulting in a 50%, 90% and 99% decrease in parasitemia relative to control values. Values were determined after treatment of 5 mice with a single dose on day 1 after infection followed by FACS analysis on day 3 (72 h after infection) to determine the effective dose. Data, shown as means, are from at least two independent experiments.

[2] ETPGS formulation

[3] 7% Tween80 / 3% Ethanol formulation

Table S8. *In vivo* activity in *P. berghei* mouse model upon three-day oral dosing

compound	3 x 10 mg/kg			3 x 30 mg/kg			3 x 50 mg/kg		
	Activity (%)	Survival[3] (days)	Cure[4] (%)	Activity (%)	Survival[3] (days)	Cure[4] (%)	Activity (%)	Survival[3] (days)	Cure[4] (%)
NITD609[1]	99.9	24.4	50	99.8	29.1	90	99.6	30	100
Artesunate[2]	92	6.5	—	98	7.2	—	NT	NT	NT
Artemether[2]	99.7	13.2	—	NT	NT	—	NT	NT	NT
Mefloquine[2]	99.9	13.8	—	99.9	14	—	NT	NT	NT
Chloroquine[2]	99.3	15.4	—	98.6	18.8	—	NT	NT	NT

NT = Not Tested

[1] 0.5% MCM / 0.1% Solutol HS15 formulation (n=10 mice)

[2] 7% Tween80 / 3%Ethanol formulation (n≥10 mice)

[3] Survival of control animals: 6-7 days

[4] Cure = no parasites present at day 30

Table S9. Summary of mutations and IC_{50} values in drug-pressured and parental lines

Line	CNV[1]	SNP[1]	IC_{50} (nM)[2]	
			NITD609	NITD678
Dd2 parent	no	none	0.44 ± 0.03	21.9 ± 1.2
NITD609-R^{Dd2} clone#1	no	I398F, P990R, (D1247Y)[3]	10.9 ± 1.6	257.0 ± 22.0
NITD609-R^{Dd2} clone#2	no	T418N, P990R	3.7 ± 1.0	153.9 ± 17.2
NITD609-R^{Dd2} clone#3	no	D1247Y	3.2 ± 0.6	70.1 ± 7.2
NITD678-R^{Dd2} clone#1	yes	G223R	2.8 ± 0.7	192.9 ± 39.3
NITD678-R^{Dd2} clone#2	no	A184S, P990R	2.8 ± 0.6	162.0 ± 15.7
NITD678-R^{Dd2} clone#3	no	I203M, I263V	4.1 ± 0.9	241.1 ± 31.5

[1] CNV: copy number variation; SNP: single nucleotide polymorphism

[2] IC_{50} values are represented as means±SD and were calculated from three independent experiments performed in quadruplicate with the SYBR Green cell proliferation assay.

[3] Third mutation observed in emergent population of NITD609-R^{Dd2} clone #1

Table S10. IC_{50} values of NITD609-R^{Dd2} clones to a collection of diverse antimalarials[1]

Line	IC_{50} values (nM)[2]									
	ANI	ART	ATQ	CHX	ConA	CPA	CycA	MFQ	PYR	THG
Dd2	9.1 ± 1.0	15 ± 1.3	0.8 ± 0.1	320 ± 15	4.5 ± 0.1	3417 ± 393	32 ± 1.9	8.4 ± 1.1	>20000	905 ± 69
Clone#1	5.8 ± 2.6	13 ± 1.8	0.6 ± 0.1	287 ± 24	7.0 ± 0.5	3460 ± 90	53 ± 20	6.7 ± 1.2	>20000	813 ± 83
Clone#2	9.2 ± 1.8	18 ± 0.4	0.8 ± 0.1	310 ± 9	8.0 ± 0.7	4160 ± 104	35 ± 14	7.0 ± 0.2	>20000	1109 ± 90
Clone#3	6.4 ± 2.0	16 ± 2.0	0.6 ± 0.1	301 ± 11	7.0 ± 1.2	3240 ± 240	27 ± 9	8.0 ± 0.9	>20000	1049 ± 76

[1] Abbreviations: anisomycin (ANI), artemisinin (ART), atovaquone (ATQ), cycloheximide (CHX), concanamycin A (ConA), cyclopiazonic acid (CPA), cyclomarin A (cycA), mefloquine (MFQ), pyrimethamine (PYR), and thapsigargin (THG).

[2] IC_{50} values are represented as means±SD and were calculated from three independent experiments performed in quadruplicate with the SYBR Green cell proliferation assay.

Table S11. Summary of transgenic constructs and corresponding IC_{50} values of the spiroindolones, artemisinin and mefloquine

Line	promoter	PfATP4 mutations	IC_{50} (nM)[1]			
			NITD609	NITD678	ART	MFQ
$Dd2^{attB}$	N/A	parental	0.85 ± 0.17	39.20 ± 8.0	15.36 ± 0.89	19.85 ± 0.16
$Dd2^{attB}$	EF1-α	wild-type	0.92 ± 0.03	44.13 ± 3.7	17.16 ± 1.21	13.15 ± 2.05
$Dd2^{attB}$	EF1-α	D1247Y	1.57 ± 0.14	62.63 ± 3.1	19.78 ± 0.31	12.50 ± 1.78
$Dd2^{attB}$	EF1-α	I398F/P990R	1.89 ± 0.06	68.74 ± 4.3	17.34 ± 1.14	14.07 ± 0.33
$Dd2^{attB}$	CAM	D1247Y	3.90 ± 0.65	81.02 ± 7.2	16.25 ± 1.3	11.04 ± 0.87
$Dd2^{attB}$	CAM	I398F/P990R	4.25 ± 0.54	109.9 ± 13.0	17.96 ± 0.39	12.87 ± 0.53

[1] IC_{50} values are represented as means±SD and were calculated from three independent experiments performed in quadruplicate with the SYBR Green cell proliferation assay.

Table S12. Analysis of variance table for comparisons between compounds

	Degrees of freedom	Sum of squares	Mean square	F-statistics
Time point (4 compounds, 4 time points)	15	2590.8	172.7	282.6
Compounds concentration (4 compounds each at 7 concentrations)	24	405.6	16.9	27.5
Parasite stage by compound	8	356.0	44.5	72.8
Main effect of parasite stage (3 stages)	2	266.2	133.1	217.9
Difference between compounds in effect of parasite stage	6	89.7	15.0	24.5
Residual	935	571.3	0.61	

Table S13. Statistical tests of stage-specificity and of concentration-dependence of stage-specificity

Compound	Main effect[1]		Interaction[2]	
	F-statistic	P-value	F-statistic	P-value
NITD261	430.3	<0.0001	12.2	<0.0001
NITD609	340.9	<0.0001	3.1	0.046
Pyrimethamine	336.5	<0.0001	33.3	<0.0001
Artemether	5.6	0.004	7.1	0.001

[1] The main effect tested was the effect of the parasite stage on the log-transformed relative count, adjusted for the time point of sampling. F-statistics had 2 and 246 degrees of freedom for compounds NITD261 (see structure below in Fig. S7), NITD609 and pyrimethamine; and 2 and 221 degrees of freedom for artemether.

[2] Tested was the effect of the interaction between logarithm of the concentration and the parasite stage, adjusted for the time point of sampling, parasite stage, and the interactions between stage and time point. F-statistics had 2 and 237 degrees of freedom for compounds NITD261, NITD609 and pyrimethamine; and 2 and 212 degrees of freedom for artemether.

Supplemental Figures

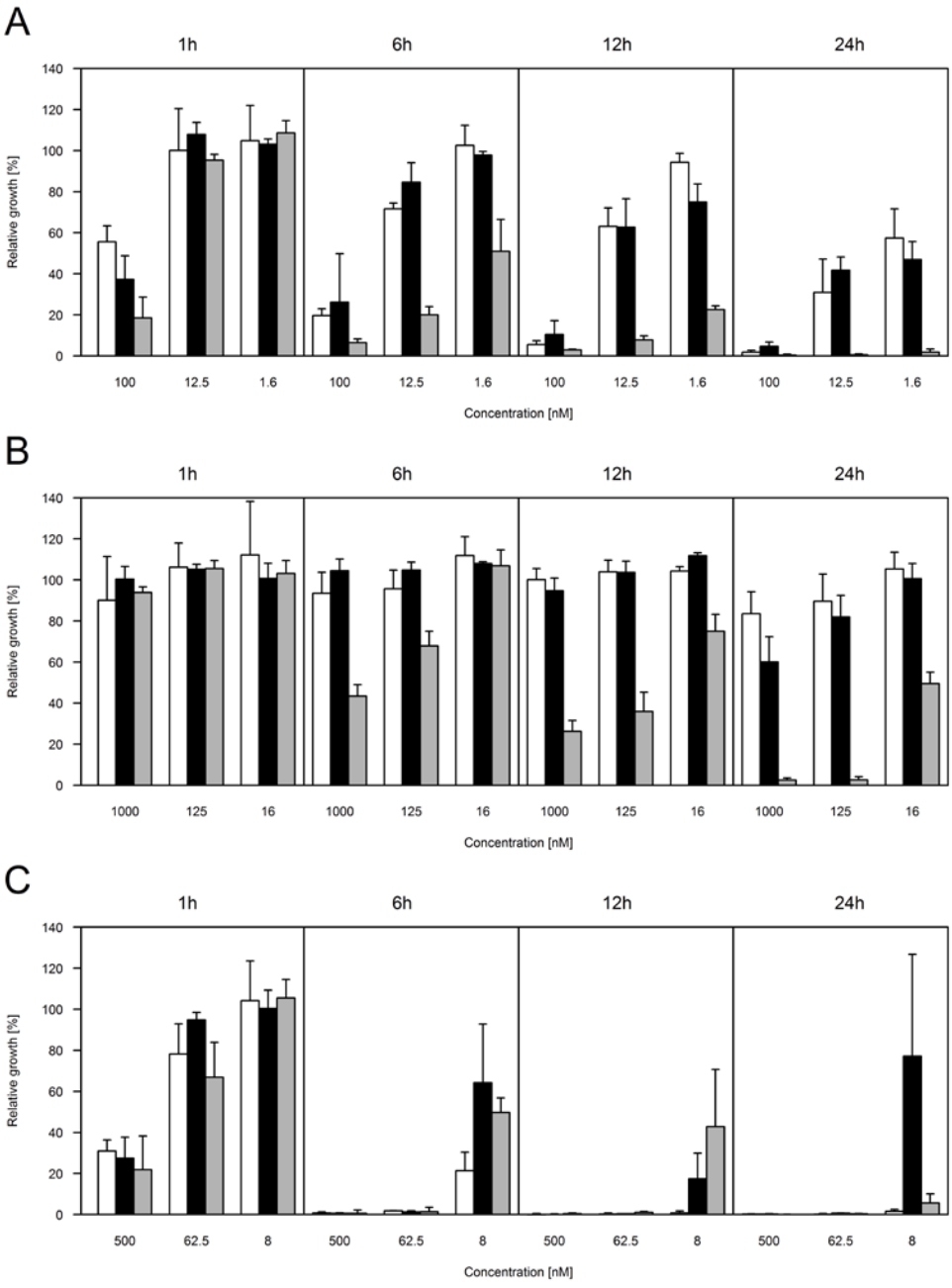

Fig. S1. Stage-dependent effects of NITD609 on *P. falciparum* parasites

Synchronous cultures of *P. falciparum* strain 3D7 were treated with 1×, 10× or 100× the respective IC_{50} values of **(A)** NITD609, **(B)** pyrimethamine, or **(C)** artemether for 1, 6, 12 or 24 h. After removal of the compounds, parasites were incubated for a further 24 h in the presence of [^{3}H]-hypoxanthine. Compound effects are expressed as the percentage of growth of the respective developmental stage relative to untreated controls (Relative growth %). White bars, ring stage; black bars, trophozoite stage; grey bars, schizont stage. Each bar represents the mean of 3 independent experiments with error bars showing the standard deviation.

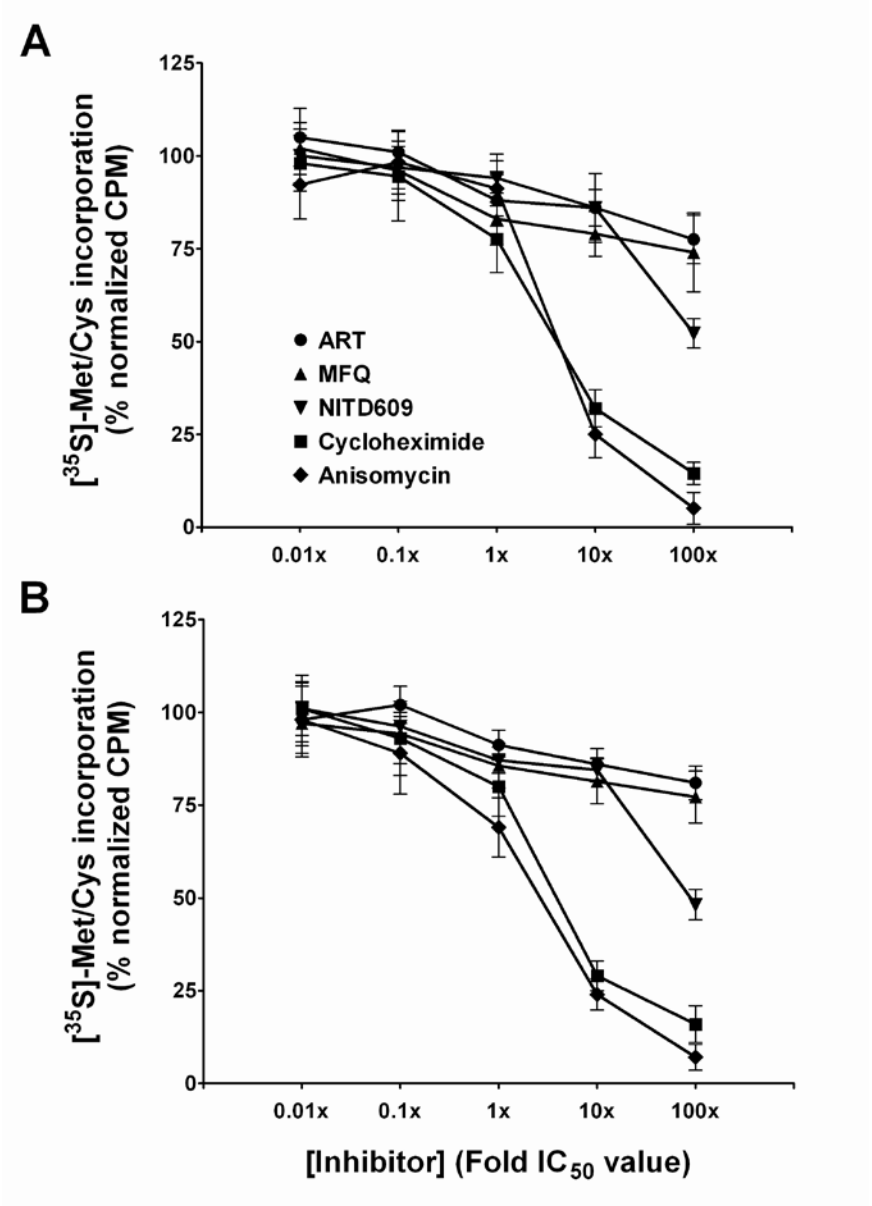

Fig. S2. Similar losses of protein synthesis inhibition upon NITD609 treatment in NITD609-R^{Dd2} clones #1 and #3

The rate of parasite protein synthesis was evaluated by monitoring [^{35}S]-radiolabelled methionine and cysteine ([^{35}S]-Met/Cys) incorporation into asynchronous cultures. Parasites were assayed for 1 hour in the presence of NITD609 (inverted triangle), anisomycin (diamond), cycloheximide (square), artemisinin (circle), or mefloquine (triangle), then extracted for radiographic measurements. Radiolabel incorporation was measured against inhibitor dosed over a five-log concentration range and percent incorporation was calculated by comparison to cultures assayed in the absence of inhibitor. Anisomycin and cycloheximide were included as positive controls. **(A)** NITD609-R^{Dd2} clone #1 and **(B)** NITD609-R^{Dd2} clone #3 reverse the protein synthesis inhibition phenotype associated with NITD609-treated Dd2 wild-type. Whereas 50% inhibition of [^{35}S]-Met/Cys incorporation was observed with 3x NITD609 IC_{50} in Dd2, 100× and 87x NITD609 IC_{50} values were required to achieve the same inhibition in NITD609-R^{Dd2} clones #1 and #3, respectively. Data are expressed in mean±SD and represent three independent experiments performed in triplicate.

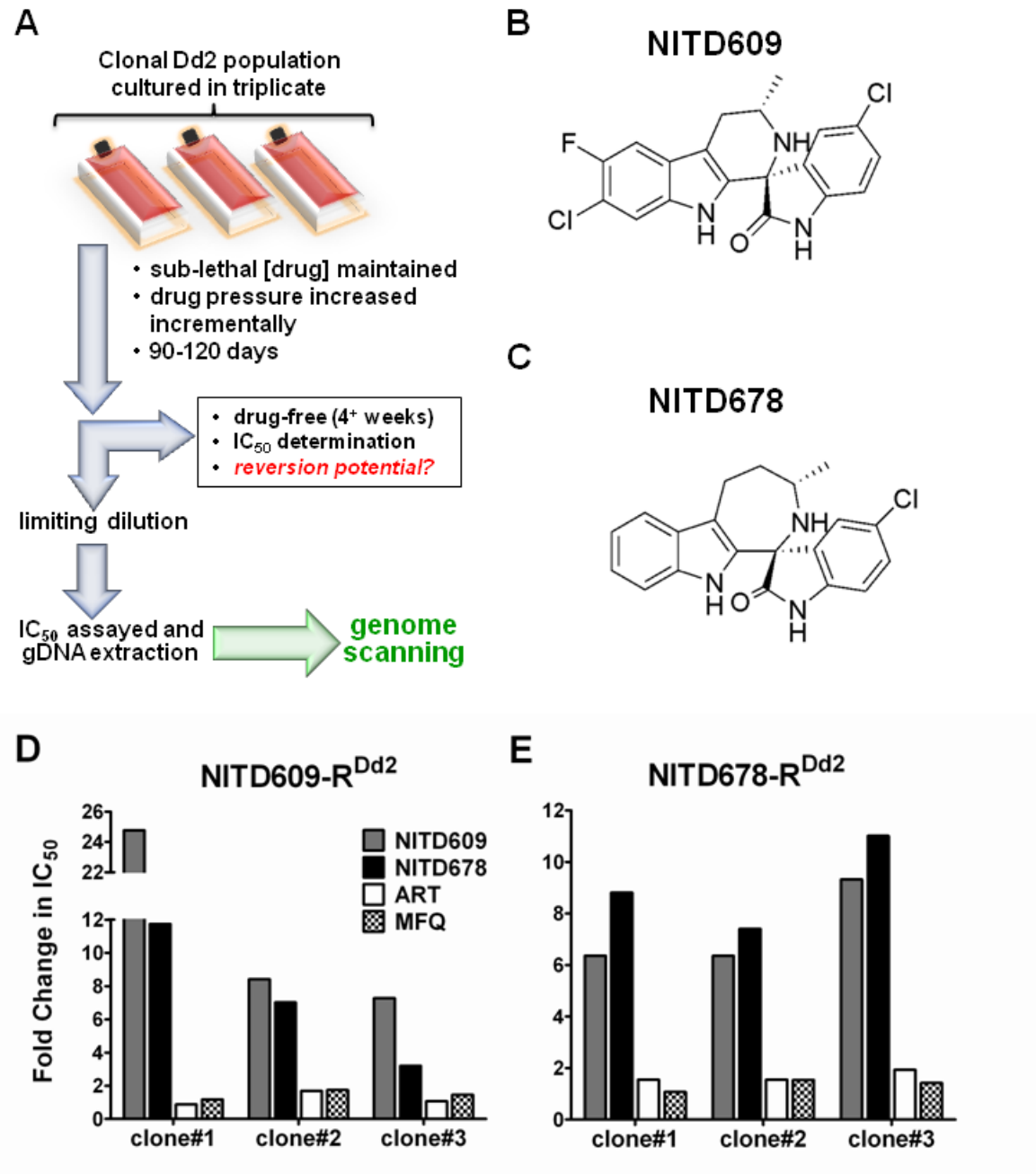

Fig S3. Evolution of spiroindolone-resistant parasites

(A) Schematic representation of the methodology used to select and analyze drug-resistant parasites. **(B)** Chemical structure of NITD609. **(C)** Chemical structure of NITD678, a less potent analog of NITD609. **(D)** NITD609-R^{Dd2} and **(E)** NITD678-R^{Dd2} clones were assayed to determine the fold change in IC_{50} value for both spiroindolones, artemisinin (ART) and mefloquine (MFQ) in comparison to the parental Dd2 strain. Absolute IC_{50} values of spiroindolones are given in Table S9. Predictably, the spiroindolones demonstrated cross-resistance, whereas little or no change in potency is observed for the antimalarials artemisinin (ART) and mefloquine (MFQ).

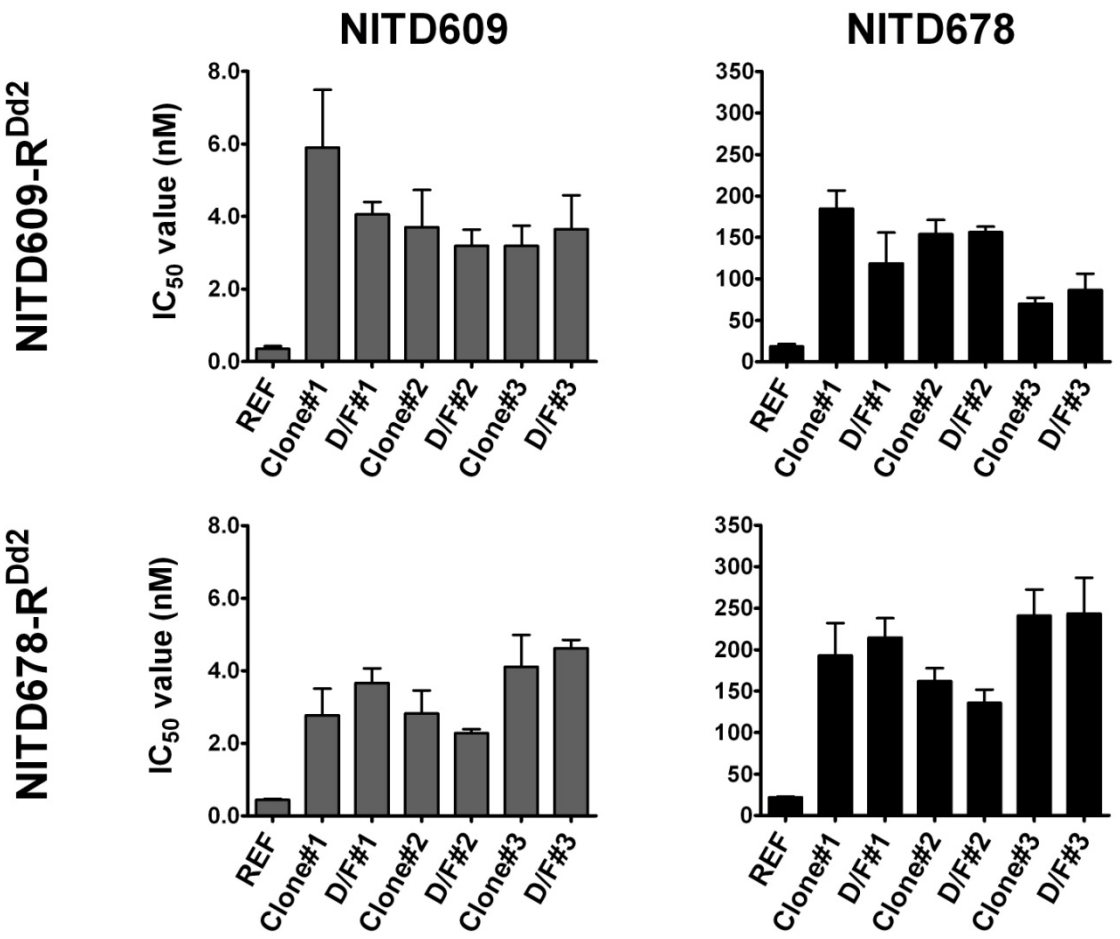

Fig. S4. Drug resistance was stably acquired in each of the resistant lines

After 4 months of drug-free culturing, each resistant line was re-evaluated for drug sensitivity using the SYBR Green cell proliferation assay. Values are presented as the mean±SD derived from three independent experiments performed in duplicate. Resistant lines cultured under drug-free conditions (D/F designation) largely showed the same IC_{50} as the original clones and retained cross-resistance to both spiroindolones. The exception was NITD609-R^{Dd2} clone #1, which showed a reduction in IC_{50}, likely due to an emergent population of mixed genetic background. However, even this emergent line still retained some degree of resistance. These data suggest that the SNPs in *pfatp4* do not confer a significant fitness cost to the parasite that results in rapid reversion to the parental phenotype.

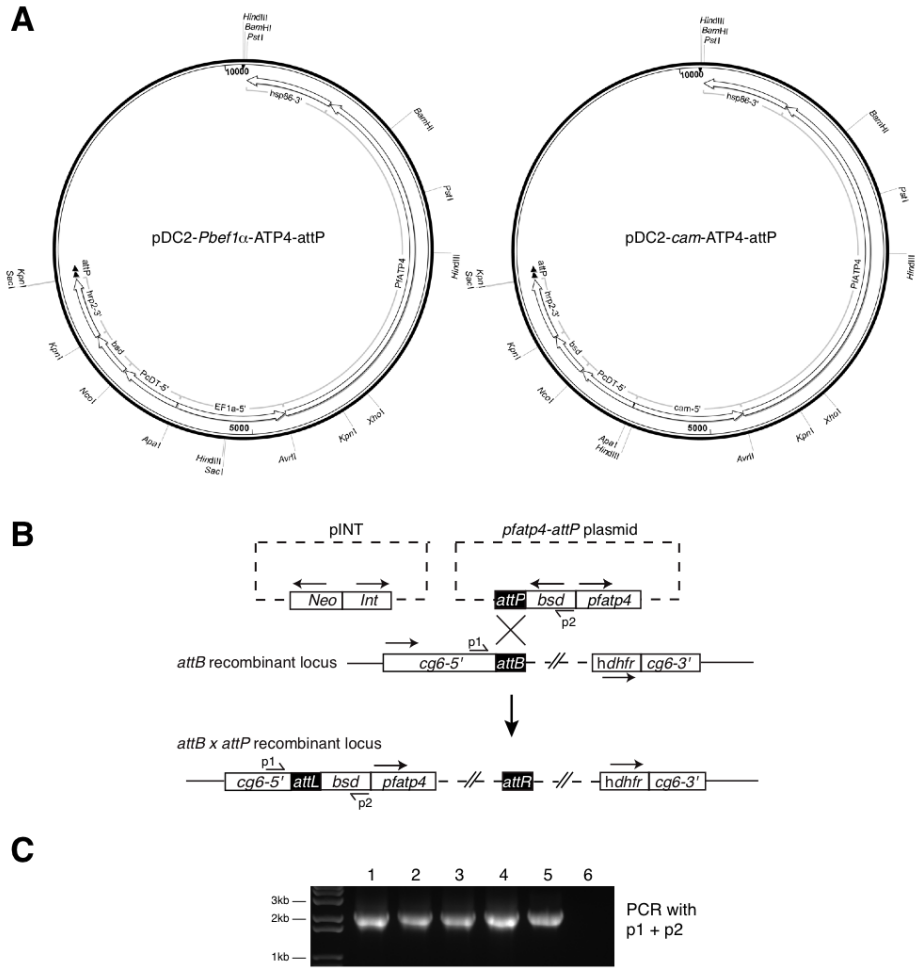

Fig. S5. Generation of transgenic parasites expressing PfATP4 by integrase-mediated recombination

(A) Plasmid maps of the attP-containing PfATP4 expression vectors. The *pfatp4* transgene was placed under the control of either the *P. berghei EF1*α 5'UTR or the *P. falciparum* 1kb *calmodulin* 5'UTR. **(B)** Schematic representation of the recombination event between a *pfatp4*-attP plasmid and an attB site located within the *cg6* locus of Dd2. Recombination is driven by coexpression of the mycobacteriophage Bxb1 integrase supplied on an additional plasmid, pINT. Primers located within the *cg6* locus (p1: 5'-GAAAATATTATTACAAAGGGTGAGG) and the blasticin S-deaminase (*bsd*) selectable marker cassette (p2: 5'-ACGAATTCTTAGCTAATTCGCTTGTAAGA) were used to amplify the attB-attP recombinant locus. **(C)** PCR amplification using primers p1 and p2 was performed on genomic DNA isolated from either the *pfatp4* transgenic lines or the Dd2^{attB} parental line. Parasite lines were transfected with *PbEF1*α-driven wild-type *pfatp4* (lane 1), the (I398F, P990R) double mutant (lane 2), the D1247Y) single mutant (lane 3), the *Pfcam*-driven (I398F, P990R) double mutant (lane 4), the *Pfcam*-driven (D1247Y) single mutant (lane 5), or untransfected parental Dd2^{attB} (lane 6).

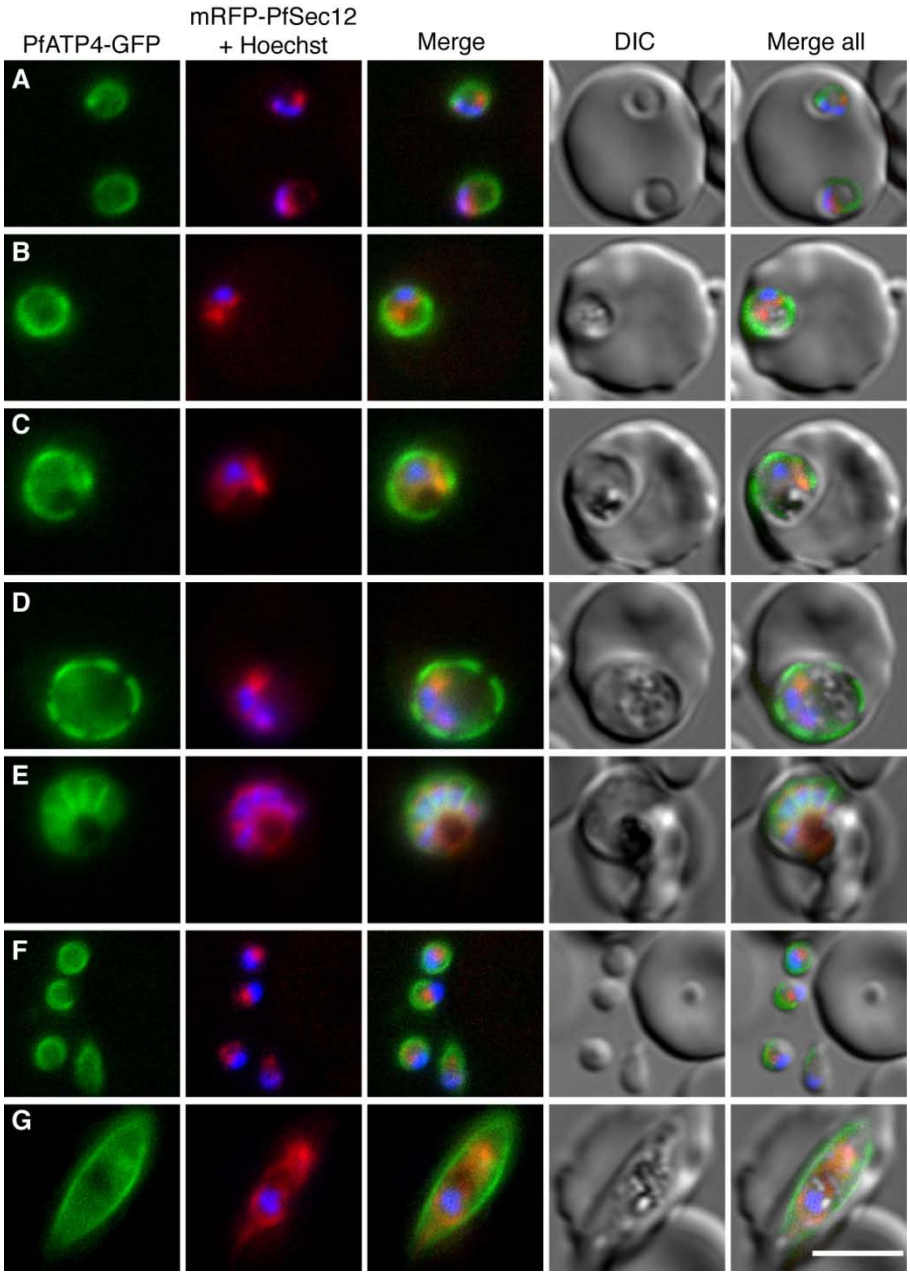

Fig S6. PfATP4 localizes to the parasite plasma membrane

Live-cell imaging of transgenic parasites co-expressing PfATP4-GFP (green) and an ER marker, mRFP-PfSec12 (red). Parasites were labeled with Hoechst 33382 to visualize the nucleus (blue). PfATP4-GFP was observed at the parasite plasma membrane at all stages of the intraerythrocytic lifecycle, including **(A)** ring stage, **(B)** early trophozoite, **(C)** mature trophozoite, **(D)** early schizont (two nuclei), **(E)** late segmented schizont, **(F)** free merozoites, and **(G)** gametocyte, the sexual intra-erythrocytic form of the parasite. Bar = 5 µm.

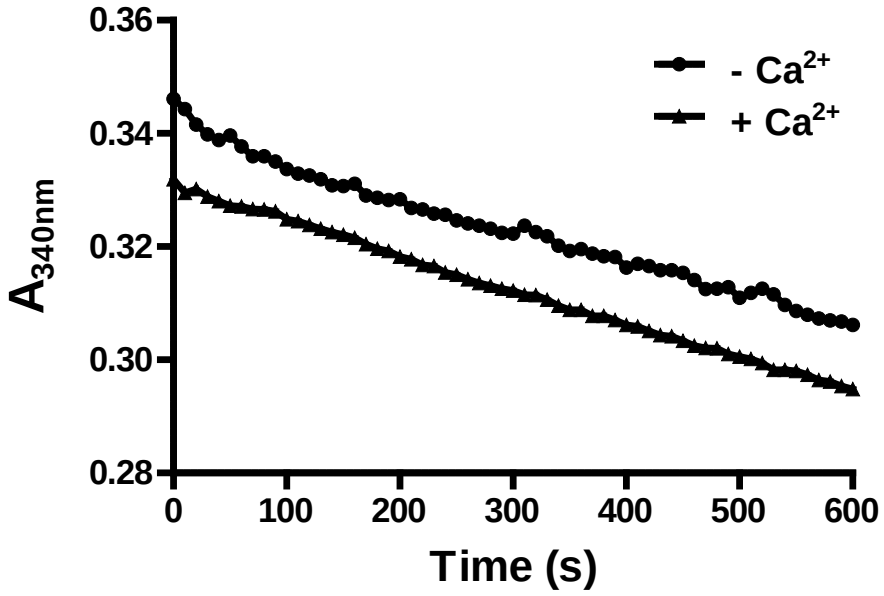

Fig. S7. Measurement of ATP hydrolysis in purified membranes from *Xenopus laevis* oocytes.

A coupled enzymatic assay with pyruvate kinase and lactate dehydrogenase was used to monitor the consumption of ATP by membranes purified from oocytes that were injected with wild-type *pfatp4* cDNA. The rate of hydrolysis was indistinguishable in the presence or absence of 25 µM $[Ca^{2+}]_{free}$ in the assay buffer. This finding suggests that no calcium-dependent ATPase activity was present in the membrane preparations and that all observed activity was derived from endogenous ATPases/kinases.

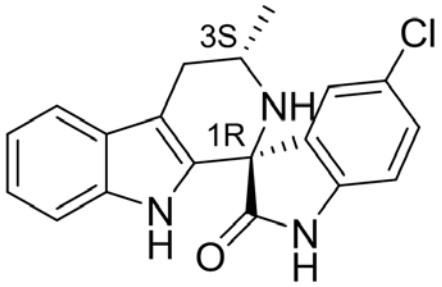

NITD261

Fig. S8. Chemical structure of NITD261

The chemical structure of NITD261, showing the 1R,3S configuration that is essential for antimalarial activity. Key physicochemical properties are: solubility (pH 6.8) 194 μg/mL; logP (pH 7.4) 3.4; logD (pH 7.4) 3.5; pKa1 5.1; pKa2 10.4; polar surface area 56.92 Å2. When compared to NITD609, NITD261 displays lower anti-plasmodium potency (NF54 IC_{50} = 9.2 nM) and limited oral bioavailability.

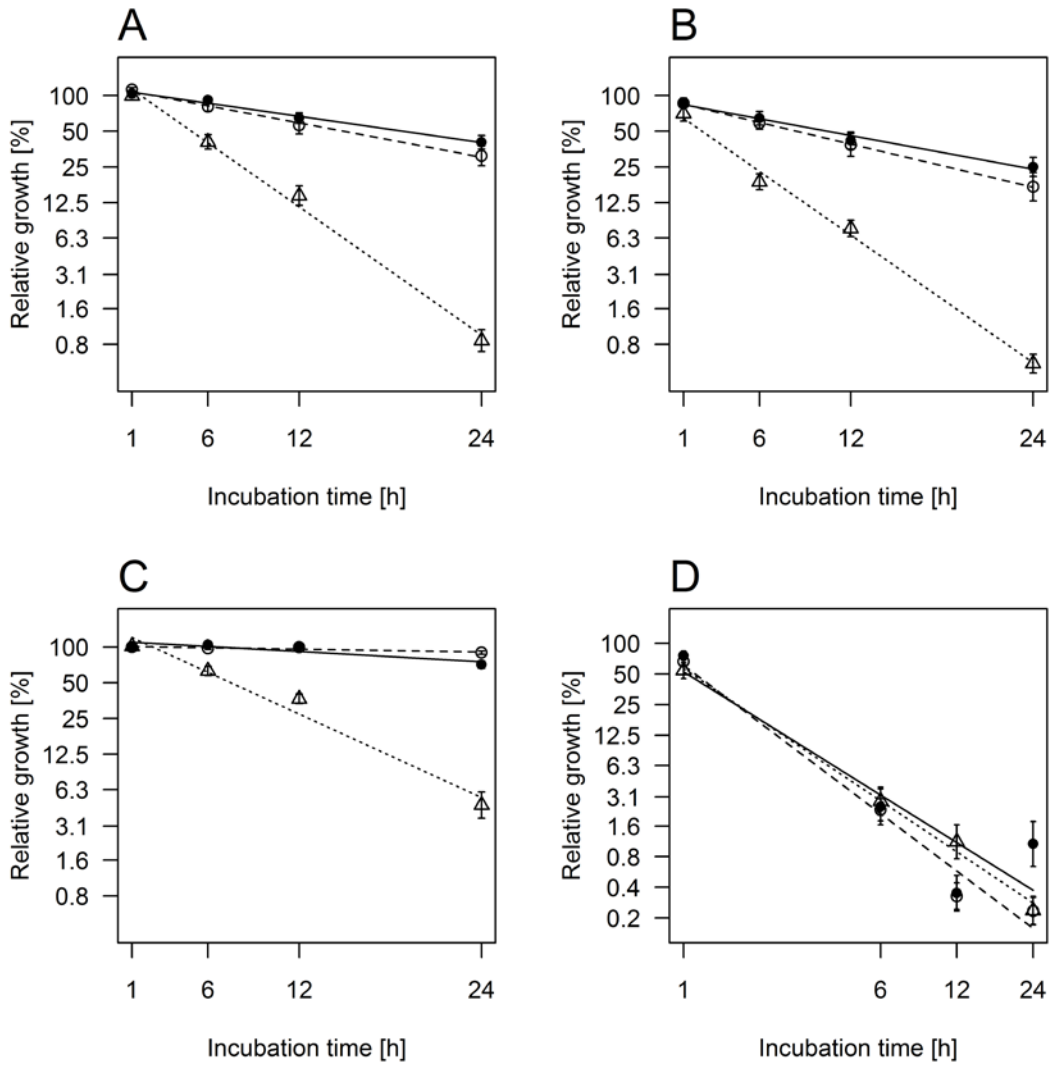

Fig S9. Time- and stage-dependent effects

(**A**) NITD261, (**B**) NITD609, (**C**) pyrimethamine and (**D**) artemether. Synchronized cultures of *P. falciparum* 3D7 (● rings, ○ trophozoites and∆ schizonts) were exposed for a 1, 6, 12 or 24 h period to antimalarial compounds (titrated over a 64 fold concentration range starting with 100 x the respective IC_{50}). Cultures were washed four times and incubated for another 24 h in the presence of 0.5µCi [^{3}H]-hypoxanthine. Compound effects are expressed as the percentage of growth of the respective development stage relative to untreated controls (Relative growth [%]). To analyze time and stage-specificity individual linear models for all stages were fitted to log (Relative growth [%]), as a function of incubation time (Artemether: linear model fitted to log (Relative growth [%] as a function of the log incubation time) averaged over all concentrations. Error bars are ± standard error of the mean of the data on a logarithmic scale. All parasite stages were highly susceptible to the spiroindolones NITD261 (**A**) and NITD609 (B) although schizonts (∆) were killed faster and more efficiently. Pyrimethamine (**C**) served as a control showing exclusive killing of schizonts, whereas artemether (**D**) displayed very fast stage-independent killing.

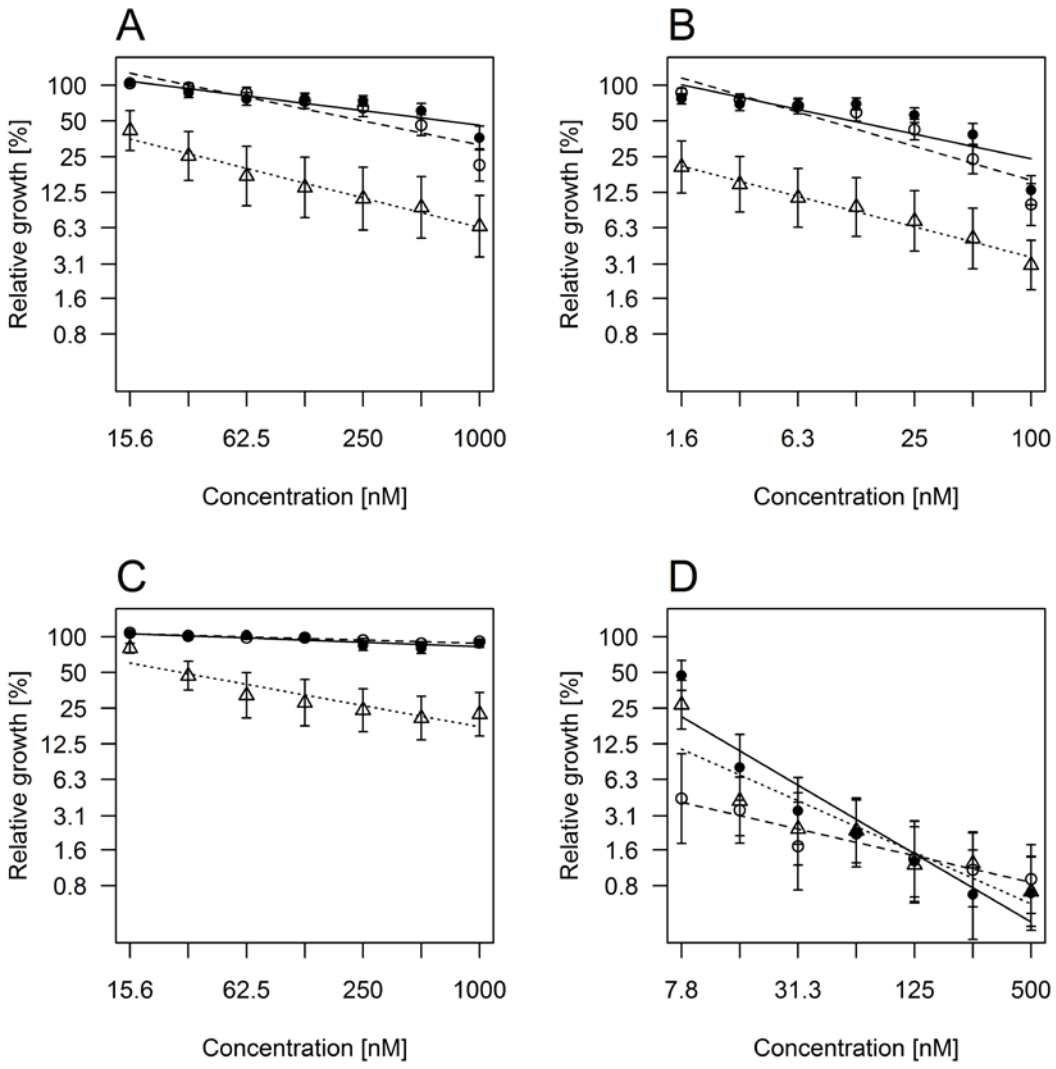

Fig S10. Concentration- and stage-dependent effects

(**A**) NITD261, (**B**) NITD609, (**C**) pyrimethamine and (**D**) artemether. Synchronized cultures of *P. falciparum* 3D7 (● rings, ○ trophozoites and∆ schizonts) were exposed for a 1, 6, 12 or 24 h period to antimalarial compounds (titrated over a 64 fold concentration range starting with 100 x the respective IC_{50}). Cultures were washed four times and incubated for a further 24 h in the presence of 0.5 µCi [^{3}H]-hypoxanthine. Compound effects are expressed as the percentage of growth of the respective developmental stage relative to untreated controls (Relative growth [%]). To analyze concentration and stage-specificity, individual linear models for all stages were fitted to log (Relative growth [%]), as a function of the logarithm of the compound concentration averaged over all timepoints. Error bars are ± standard error of the mean of the data on a logarithmic scale. All parasite stages were highly susceptible to the spiroindolones NITD261 (**A**) and NITD609 (**B**) although schizonts (∆) were killed preferentially. Pyrimethamine (**C**) served as a control showing killing of schizonts exclusively, whereas artemether (**D**) displayed stage-independent killing.

Materials and Methods

Drugs and reagents

The following formulation reagents were purchased from the indicated providers: Methyl Cellulose from Sigma, Solutol HS15 from BASF, Ethanol from Fisher, PEG400 from Acros and Vit, and ETPGS from Eastman. Standard antimalarial and control drugs were purchased from the following vendors: Chloroquine diphosphate salt from Sigma-Aldrich, artesunate from Mepha Pharma AG, artemether from Kunming Pharmaceutical Corp., mefloquine hydrochloride from Hoffmann-LaRoche Ltd, and sodium artesunate from Guilin Factory, Guangxi, China.

NITD609 SYNTHESIS

NITD609 was synthesized as a racemate and separated by chiral chromatography to provide the active 1*R*,3*S* enantiomer.

General methods. Reagents and solvents were purchased from Aldrich, Acros, or other commercial sources and used without further purification. Thin layer chromatography (TLC) was performed on precoated silica gel 60 F_{254} plates from Merck. Compounds were visualized under UV light, ninhydrin, or phosphomolybdic acid (PMA) stain. NMR spectra were obtained on a Varian 300 MHz Mercury NMR or Bruker 500 MHz Ultrashield spectrometer using $CDCl_3$, DMSO-d_6, or MeOD-d_4 as solvents. Preparative chiral separation was performed on a Chiracel OD-H column (2 x 25 cm) with 90:10 hexanes:ethanol as the mobile phase. Analytical chiral chromatography was carried out on Chiracel AD-H column and all enantiomers reported were greater than 98% enantiomeric excess (e.e.). Purity of all compounds were determined by LC/MS and HPLC and determined on an Agilent LC1100 HPLC equipped with a Waters Symmetry Shield RP18, 3.5 μm, 4.6 x 150 mm column using a gradient (13 minutes) of 95:5 0.1% formic acid in water:CH_3CN to 95:5 CH_3CN:0.1% formic acid in water. The purity of all reported compounds was >95% at 254 nm. Optical rotation of the single enantiomers was measured on a Jasco P-1020 polarimeter at 25°C.

5',7-Dichloro-6-fluoro-3-methyl-2,3,4,9-tetrahydrospiro[β-carboline-1,3'-indol]-2'(1'*H*)-one: Phosphorous oxychloride (2.43 mL, 26.5 mmol) was added dropwise to dry DMF (15.0 mL) at –20°C and stirred at –5°C. After one hour, a solution of 6-chloro-5-fluoroindole (3.0 g, 17.7 mmol) in dry DMF (5.0 mL) was added dropwise to the above mixture at –20°C. After addition, the cooling bath was removed and the reaction mixture allowed to warm to room temperature and then heated to 35°C. After one hour, the reaction was poured onto ice and basified with solid sodium bicarbonate and washed with ethyl acetate. The combined organic layers were washed with water, dried over sodium sulfate, and concentrated in vacuo to give 6-chloro-5-fluoro-1*H*-indole-3-carbaldehyde (3.4 g, 97%) as a light brown solid. ^{1}H NMR (500 MHz, $CDCl_3$): δ 10.02 (s, 1H), 8.10 (d, *J* = 9.5 Hz, 1H), 7.87 (s, 1H), 7.49 (d, *J* = 5.5 Hz, 1H).

A 0.2 M solution of 6-chloro-5-fluoro-1*H*-indole-3-carbaldehyde (4.0 g, 20.24 mmol) in nitroethane (100 mL) was refluxed with ammonium acetate (1.32 g, 0.85 mmol). After 4 hours, the reaction mixture was concentrated in vacuo to remove nitroethane, diluted with ethyl acetate and washed with brine. The organic layer was concentrated to provide 6-chloro-5-fluoro-3-(2-nitro-propenyl)-1*H*-indole (5.0 g, 97%) as a red-orange solid. ^{1}H NMR (500 MHz, $CDCl_3$): δ 8.77 (s, 1H), 8.32 (s, 1H), 7.58 (d, *J* = 2.5 Hz, 1H), 7.54 (d, *J* = 9.0 Hz, 1H), 7.50 (d, *J* = 5.9 Hz, 1H), 2.52 (s, 3H).

A solution of 6-chloro-5-fluoro-3-(2-nitro-propenyl)-1*H*-indole (5.0 g, 19.6 mmol) in dry THF (10 mL) was added to the suspension of lithium aluminum hydride (2.92 g, 78.5 mmol) in THF (20 mL) at 0°C and then heated to reflux for 3 hours. The reaction mixture was cooled to 0°C, and quenched by slow addition of water and 5% aqueous NaOH. The reaction mixture was filtered through Celite and the filtrate concentrated to give 2-(6-chloro-5-fluoro-1*H*-indol-3-yl)-1-methyl-ethylamine (4.7 g crude) as a viscous brown liquid. The residue was used without further purification. ^{1}H NMR (500 MHz, $CDCl_3$): δ 8.13 (s, 1H), 7.37 (d, *J* = 6.0 Hz, 1H), 7.32 (d, 1H, *J* = 10.0 Hz), 7.08 (s, 1H), 3.23-3.26 (m, 1H), 2.77-2.81 (m, 1H), 2.58-2.63 (m, 1H), 1.15 (d, *J* = 6.5 Hz, 3H).

A mixture of 2-(6-chloro-5-fluoro-1*H*-indol-3-yl)-1-methyl-ethylamine (4.7 g, 20.7 mmol), 5-chloroisatin (3.76 g, 20.7 mmol) and *p*-toluenesulfonic acid (394 mg, 2.07 mmol) in ethanol (75 mL) was refluxed overnight. The reaction mixture was concentrated in vacuo, diluted with ethyl acetate and washed with saturated aqueous $NaHCO_3$. The organic layer was concentrated to give a brown residue, which was purified by silica gel chromatography (20% EtOAc in hexane) to provide racemic NITD609 (4.5 g, 56%) as a light yellow solid. ^{1}H NMR (500 MHz, DMSO-d_6): δ 10.69 (s,1H), 10.51 (s,1H), 7.43 (m, 1H), 7.32 (d, *J* = 8.3 Hz, 1H), 7.26 (m, 1H), 7.04 (s, 1H), 6.93 (d, *J* = 8.3 Hz, 1H), 3.91 (m, 1H), 3.12 (bd, *J* = 5.5 Hz, 1H), 2.77 (bd, *J* = 14.2 Hz, 1H), 2.38 (dd, *J* = 14.2, 10.9 Hz, 1H), 1.16 (d, *J* = 6.5 Hz, 1H); MS (ESI) *m/z* 390.0 $(M)^+$. The racemate was separated into its enantiomers by chiral chromatography under the conditions described in general methods. Note: The Pictet-Spengler cyclization for this reaction was found to be highly diastereoselective and preferentially formed the 1*R*,3*S* and 1*S*,3*R* stereoisomers over the 1*R*,3*R* and 1*S*,3*S* pair in ~ 9:1 ratio under the reaction conditions.

(1*R*,3*S*)-5',7-dichloro-6-fluoro-3-methyl-2,3,4,9-tetrahydrospiro[β-carboline-1,3'-indol-2'(1'*H*)-one (NITD609): ^{1}H NMR (500 MHz, DMSO-d_6): δ 10.69 (s, 1H), 10.51 (s, 1H), 7.43 (d, *J* = 10.0 Hz, 1H), 7.33 (dd, *J* = 8.4, 2.2 Hz, 1H), 7.27 (d, *J* = 6.5 Hz, 1H), 7.05 (d, *J* = 2.3 Hz, 1H), 6.93 (d, *J* = 8.5 Hz, 1H), 3.91 (m, 1H), 3.13 (bd, *J* = 6.2 Hz, 1H), 2.74 (dd, *J* = 15.0, 3.0 Hz, 1H), 2.35 (dd, *J* = 15.0, 10.3 Hz, 1H), 1.15 (d, *J* = 6.0 Hz, 3H); MS (ESI) *m/z* 392.0 $(M+2H)^+$; HRMS (ESI) for $C_{19}H_{15}Cl_2FN_3O$ $(M+H)^+$ calculated 390.0571, found 390.0556; $[\alpha]_D^{25}$ = +255.4° (*c* = 0.10 g/mL, methanol).

***In vitro* antimalarial activity and stage/rate of action studies**

Isolates of *P. falciparum* were maintained by standard methods (S*2*) in an atmosphere of 93% N_2, 4% CO_2, 3% O_2 at 37°C in complete medium (CM: RPMI 1640 10.44 g/L, Hepes 5.94 g/L, Albumax II 5 g/L, hypoxanthine 50 mg/L, sodium bicarbonate 2.1 g/L and neomycin 100 mg/L). Human erythrocytes served as host cells. *In vitro* antimalarial activity was measured using the [^{3}H]-hypoxanthine incorporation assay (S*3*) with selected strains of *P. falciparum* (NF54 was obtained from Hoffmann-LaRoche Ltd., 3D7, K1, W2, 7G8, TM91C235, D6 and V1/S were obtained from MR4). Compounds were dissolved in DMSO (10 mM), diluted in hypoxanthine-free culture medium and titrated in duplicates over a 64 fold range in 96-well plates. Infected erythrocytes (0.3% final parasitemia and 1.25% final hematocrit) were added into the wells. After 48 h incubation, 0.5 µCi of [^{3}H]-hypoxanthine was added per well and plates were incubated for an additional 24 h. Parasites were harvested onto glass-fiber filters and radioactivity was counted using a Betaplate liquid scintillation counter (Wallac, Zurich). Results were recorded and expressed as a percentage of the untreated controls. Fifty percent inhibitory concentrations (IC_{50}) were estimated by linear interpolation. For stage and rate of action studies parasites were synchronized twice (8 hours apart) with 5% D-sorbitol (S*4*). Determination of stage-specificity was carried out with strain 3D7 as previously

described (S*5*). Briefly, synchronized cultures (0.15% final parasitemia and a 2.5% final hematocrit) were exposed for a 1, 6, 12 or 24 h period to antimalarial compounds (titrated in duplicates over a 64 fold range in 96-well plates with a starting concentration of 100 fold the respective IC_{50}). After the relevant incubation times the plates were washed four times and incubated for a further 24 h in the presence of 0.5 µCi [^{3}H]-hypoxanthine per well. Plates were frozen at –20 °C, thawed, harvested onto glass filters, radioactivity was counted using a Betaplate liquid scintillation counter (Wallac, Zurich) and expressed as a percentage of the untreated controls. All assays were repeated at least three times.

STATISTICAL METHODS

The response analyzed was the relative growth (*Y*). To analyze stage-specificity of antimalarial compounds, linear models were fitted to log(*Y*) including separate terms for each compound, and within each compound for each concentration, each time point, and each parasite stage. The effect of parasite stage was analyzed into two components: the main effect of each stage, common to all four compounds (accounting for two degrees of freedom) and the difference between compounds in the effect of parasite stage (6 degrees of freedom). The variation accounted for by each of these components was compared with the residual variation using F-tests (see Table S12 and S13 above) to analyze whether the stage-specificity was dependent on compound.

RESULTS OF STATISTICAL ANALYSIS

The effects tested in the comparison between compounds were all highly statistically significant (Table S12). In particular, the F-statistics testing whether the overall effect of compound treatment was stage-specific ($F_{2,935}$ = 217.9, P<0.0001) and that testing whether the stage-specificity differs by compound ($F_{6,935}$ = 24.5, P<0.0001).

Similarly, the statistical tests of whether the compound effects were stage-specific all gave low P-values (Table S13), although the stage-specificity for artemether was clearly much less than for the other compounds. This is illustrated by the fact that the curves for the different stages in Figure S10D cross over, and the F-statistic testing the main effect of stage-specificity is much lower for artemether than for the others (Table S13).

Each of the four compounds examined had different concentration dependence of the effects, although the patterns for compounds NITD261 (Fig S8) and NITD609 were very similar. Both compounds killed schizonts at lower concentrations than the minimum tested, hence the heavy lines in Fig S9A-B and Fig S10A-B are well below the lines for trophozoites and ring stages. However compound NITD609 (Fig S10B) is clearly effective at much lower concentrations than compound NITD261 (Fig S10A—note the difference in the horizontal scales). The concentration curves for ring and trophozoite stages for these two compounds are very similar to each other, and approximately parallel with the curves for schizonts in Fig S9A-B and Fig S10A-B, implying that at high concentrations the other stages are killed in proportion to the killing of schizonts.

Pyrimethamine almost exclusively killed schizonts (Fig S9C and Fig S10C concentration curves for rings and trophozoites both indicated that there was little or no killing of other stages).

The pattern for artemether was very different from that of any of the other compounds (Fig S9D and Fig S10D). The formal statistical test of stage-specificity in the killing effect was significant, but this difference was clearly much less for this drug than for the others. Moreover the concentration dependence in the killing effect was very similar for all stages.

In vivo antimalarial activity

All *in vivo* efficacy studies were approved by the veterinary authorities of the Canton Basel-Stadt. *In vivo* antimalarial activity was usually assessed for groups of five female NMRI mice (20–22 g) intravenously infected on day zero with $2x10^7$ erythrocytes parasitized with *P. berghei* GFP ANKA malaria strain ($PbGFP_{CON}$ donation from AP Waters and CJ Janse, Leiden University (S*6*)). Untreated control mice die typically between day six and day seven post infection. Experimental compounds were formulated in 10% Ethanol, 30% PEG400 and 60% of 10% Vitamin E (ETPGS) or in the case of crystalline material in 0.5% Methylcellulose and 0.1% Solutol HS15. Compounds were administered orally in a volume of 10 mL/kg either as a single dose (24 h post infection) or as three consecutive daily doses (24, 48 and 72 h post infection). With the single dose regimen parasitemia was determined (72 h post infection) and for the triple dose regimen (96 h post infection) using standard flow cytometry techniques (S*6*). Activity was calculated as the difference between the mean percent parasitemia for the control and treated groups expressed as a percentage of the control group. The survival time in days was also recorded up to 30 days after infection. A compound was considered curative if the animal survived to day 30 after infection with no detectable parasites.

Ex vivo P. falciparum and *P. vivax* maturation assays

Ten *P. vivax* and ten *P. falciparum* isolates were collected from the Mae Sot region of Tak Province (Thailand) in 2009. All samples were collected from patients with acute malaria (with a mono species parasitemia of 2000-10,000 parasites/µL) attending the clinics of Shoklo Malaria Research Unit. After obtaining written consent, blood samples were collected by venipuncture onto heparinized tubes and were processed within 5 h of collection at room temperature. Samples with more than 80% early trophozoites were chosen for drug sensitivity testing. After platelets and leukocytes were removed from the isolates (S*7*), the sensitivity of the *P. vivax* parasites was tested as previously described (S*8, 9*). Stage-specific drug activity assays were also performed as previously described (S*10*). Plates were quality controlled by testing with a strain of *P. falciparum* (K1) with a known sensitivity profile. Dose response curves and IC_{50} (50% inhibitory concentration) values were calculated by fitting the data to a sigmoidal inhibitory E-max pharmacodynamic model using WINNONLIN Ver 4.1 (Pharsight Corporation). Final IC_{50} values (in nM) were determined from the drug salt concentration of the drug. The median IC_{50} values were compared non-parametrically using the Kruskal-Wallis test. Statistical analysis and graphics were carried out using GraphPad Prism 5 software (version 5).

Metabolic labeling with [^{35}S]-methione and [^{35}S]-cysteine for protein synthesis inhibition studies

A metabolic labeling assay was developed for a 96-well format to allow for the simultaneous measurement of [^{35}S]-Met/Cys incorporation into parasites treated with numerous compounds dosed over a 5-log concentration range. Briefly, asynchronous cultures of *P. falciparum* strain Dd2 were harvested at a parasitemia of 8-10% (hematocrit of 5%), washed three times in methionine- and cysteine-free culturing media, and aliquoted in triplicate. Stock solutions, aside from NITD609, were prepared with powders purchased from Sigma and dissolved in DMSO as 1000x stock solutions. All stock solutions were based on the following IC_{50} values determined by the SYBR Green-based proliferation assay (S*11*): anisomycin (25 nM), cycloheximide (200 nM), artemisinin (15 nM), mefloquine (8 nM), and NITD609 (500 pM). Compounds were transferred to their respective parasite aliquots and preincubated for 15 minutes at 37°C

before the addition of EasyTag™ EXPRESS ^{35}S protein labeling mix (Perkin Elmer, USA) to a final concentration of 125 µCi/mL. Following a 1 h pulse at 37°C, the media was exchanged with chilled PBS supplemented with 1 mg/mL methionine and 2 mg/mL cysteine. The remaining steps were performed on ice or at 4°C when possible. The parasites were then extracted by the saponin lysis method and resuspended in PBS supplemented with 0.02% deoxycholate. TCA was immediately added to a final concentration of 8% and the resultant precipitate suspensions were transferred to a MultiScreenHTS plate with 1.2 µm FC glass and 0.65 µm Durapore membranes (Millipore, USA). The plates were washed twice with 8% TCA and a final wash of 90% acetone. The plates were air dried at room temperature and 40 µL MicroScint-20 (Perkin Elmer, USA) was added to each well. A TopCount microplate scintillation counter (Perkin Elmer, USA) was used to analyze the plates. All data were normalized to TCA precipitates from untreated parasites.

In vivo pharmacokinetic studies

The compounds were formulated at a concentration of 2.5 mg/mL for a dose of 25 mg/kg administered orally (p.o.) and of 1 mg/mL for a dose of 5 mg/kg injected intravenously (i.v.). The formulation for both p.o. and i.v. dosing was made of 10% ethanol, 30% PEG 400, and 60% of 10% Vitamin E (ETPGS). The compounds were soluble in this vehicle and were administered as a solution via both p.o. and i.v. routes. Blood samples were collected at 9 timepoints between 0 and 24 h post dosing. Groups of three animals were used for each time point. Plasma concentrations of NITD609 were measured using liquid chromatography (Agilent Zorbax Phenyl 4.6 x 75mm, 3.5mm column) coupled with tandem mass spectrometry, using an Agilent Technologies (Santa Clara, CA, USA) 1100 HPLC system and Sciex Applied Biosystems (Foster City, CA, USA) API3200 triple quadrupole mass spectrometer. Pharmacokinetic parameters were calculated using a non-compartmental approach with the WinNonLin software and methods.

In vitro metabolic stability studies

The metabolic stability in liver microsomes was determined using the compound depletion approach, quantified by LC/MS. The assay measures the rate and extent of metabolism as determined by the disappearance of the parent compound, which allows the determination of *in vitro* half life ($t_{1/2}$), intrinsic clearance (Cl_{int}) and the prediction of metabolic clearance (CL_h) in various species (S*12, 13*).

In vitro safety assessment

The cytotoxicity assay was performed as follows. Four different cell lines namely C6 Glioma (Rat brain glioma cells, adherent), THP-1 (Human monocyte, suspension), HepG2 (Human liver carcinoma, adherent) and BHK21 (Syrian Golden hamster kidney cells, adherent) were incubated with compound at varying concentrations for a period of 4 days in 96-well plates. The viability of the cells was determined by adding an XTT (2,3-bis-(2-methoxy 4-nitro 5-sulfophenyl) 2H- tetrazolium 5-carboxailide) indicator and measuring the absorbance at 450 nm. Cardiotoxicity and genotoxicity risk was measured as previously described (S*14, 15*). All assays for binding to proteins known to bear potential safety liabilities in humans were high-throughput competitive binding assays using specific radiolabeled ligands.

Toxicology study

NITD609 was dissolved in 90 volume parts of 50 mM citrate buffer at pH 3 and 10 volume parts of 1% Solutol HS15 (BASF) and administered to 5 male rats at a daily oral dose of 10 mg/kg/day (by gavage). Five control animals were treated with vehicle only.

Animals (Wistar rats; Harlan Laboratories Ltd., Horst, Netherlands) were approximately 10 weeks of age (287 to 344 g) at the start of dosing. Clinical observations, body weight and food consumption determinations, clinical pathology (hematology and clinical chemistry) evaluations, and gross pathology examinations with organ weight determinations were performed. Microscopic examinations were conducted for treated and untreated animals on all major functional organs and tissues, including but not limited to, liver, stomach, small and large intestine, thyroid/parathyroid gland, spleen, thymus, mesenteric and mandibular lymph nodes, adrenal glands, testes and epididymides. At day 1 and day 14 blood samples were collected for toxicokinetic analyses.

Selection of drug-resistant parasites

A clonal stock of the *P. falciparum* line Dd2 (parental clone) was established by limiting dilution from a Dd2 isolate (MRA-156) obtained from the Malaria Research and Reference Reagent Resource Center (MR4; American Type Culture Collection, Manassas, VA, USA), and used throughout these studies. All *P. falciparum* parasites were cultured in human erythrocytes and complete culturing media (CM) as previously described (S*11*). For each compound, the clonal Dd2 parasites were established in triplicate flasks and evolved independently. Drug challenge was initiated at the IC_{50} value for each compound in cultures with a starting parasitemia of 1-2% in 2.5% hematocrit. Cultures were observed daily by Giemsa staining of thin blood smears and culturing media supplemented with drug was changed every 1-2 days. Cultures reaching a parasitemia of 8-10%, and exhibiting a restored rate of replication, were diluted back to 1-2% parasitemia. This was deemed a successful round of challenge and was immediately followed by an incremental increase in drug pressure (10-30pM steps for NITD609-evolved clones and 10-50nM steps for NITD678-evolved clones). The continuous exposure and challenge to sub-lethal concentrations of inhibitor was carried out for 3-4 months. Frozen stocks were collected every 4-6 weeks and care was taken to make sure the DMSO concentration never exceeded 0.09% v/v in the culturing media. Each clone was tested against a panel of antimalarial compounds, and the IC_{50} values were determined by the 72h SYBR Green-based proliferation assay as described by Plouffe et al *(S11)*.

Genomic DNA analysis

Clones were selected by limiting dilution and genomic DNA was recovered from each for high-density tiling array analysis. The samples were treated as previously described by Dharia *et al*. (S*16*). In brief, genomic DNA was isolated by standard phenol-chloroform extraction. Fifteen micrograms of genomic DNA from each isolate and 10 ng each of Bio B, Bio C, Bio D, and Cre Affymetrix control plasmids (Affymetrix Inc., Santa Clara, CA, USA) were fragmented with DN*ase*I and end-labeled with biotin (S*16*). The samples were hybridized to the microarrays overnight at RT in Affymetrix buffers, washed, and scanned (S*17*). A comparative analysis of the hybridization data for each clone to the parental reference genome was performed with PfGenominator (freely available at http://www.scripps.edu/cb/winzeler/software/). Polymorphisms were detected using a sliding window of three overlapping probe sets. Probes that had significantly lower hybridization when compared to the reference were indicative of a polymorphism as determined by z-test using a p-value cutoff of 1×10^{-5} and a reference Dd2 hybridization. Gene copy number variation scanning was performed by calculating the $\log_2$ ratio of the mean intensity for probes to a gene divided by the mean intensity of the probes for a reference Dd2 hybridization as previously described (S*16*).

Cloning and sequencing of PfATP4

To confirm allelic differences in PFL0590c (*pfatp4*), the gene was PCR-amplified with Phusion polymerase (Finnzymes Inc., Woburn, MA, USA) from genomic DNA using primers ATGAGTTCTCAAAATAATAATAAACAGG (*pfatp4* start codon underlined) and TTAATTCTTAATAGTCATATATTTTCTTCTATATATAACC (*pfatp4* stop codon underlined) for amplification. The 3795-bp amplicon was ligated into pCR4Blunt-TOPO vector (Invitrogen, Carlsbad, CA, USA). The vector was transformed into One Shot Top10 chemically-competent cells (Invitrogen, Carlsbad, CA, USA), propagated with LB media and selected with 50µg/uL kanamycin. Multiple positive clones were selected on the basis of correct restriction endonuclease digestion patterns and sequenced (Eton Biosciences, San Diego, CA, USA). The M13 priming sites were utilized for sequencing of the 5'- and 3'-ends of the *pfatp4* gene and the following internal primers were required to achieve full sequencing coverage: TCACCACAATGTACTGTGTTAAGAAA, ATCCAACAAAAGGTTTTGAACCATGT, TACAAACATGTAGAGAAGCACAAGTT.

Construction of PfATP4 expression vectors, generation of stably transfected parasite lines and imaging of fluorescent parasites

The full-length *pfatp4* gene was PCR amplified using the forward primer CGCCTAGGATGAGTTCTCAAAATAATAATAAACAGGG (*Avr*II site underlined) and either AGATCTGTCGAC**TTA**ATTCTTAATAGTCATATATTTTCTTC (*Sal*I site underlined, stop codon in bold) or GAGAGATCTACCTCCACCATTCTTAATAGTCATATATTTTCTTC (*Bgl*II site underlined) as reverse primers for generation of expression constructs for the untagged protein or GFP-tagged fusion respectively. For expression of the untagged PfATP4 protein, PCR amplicons of *pfatp4* corresponding to either wild-type, the NITD609-R^{Dd2} clone#1 double mutant (Ile398Phe, Pro990Arg), or the NITD609-R^{Dd2} clone#3 single mutant (Asp1247Tyr) were inserted into pDC2-attP based expression vectors that permit integrase-mediated recombination between the attP-containing plasmid and an attB site inserted in the Dd2 parasite genome ((S*18*); Fig. S4B). Expression plasmids contained either the *P. berghei EF1*α 5'UTR or the *P. falciparum* 1kb *calmodulin* 5'UTR and were digested with *Avr*II-*Xho*I and ligated with the *pfatp4* products digested with *Avr*II-*Sal*I to generate the integrating vectors pDC2-*PbEF1*α-ATP4-attP and pDC2-*cam*-ATP4-attP (Fig. S4A). The plasmid to express the GFP tagged form of PfATP4 was generated by inserting the full-length *pfatp4* sequence without a stop codon in frame with the GFPmut2 coding sequence in a pDC2-GFP-BSD vector, under the control of the *P. berghei EF1*α 5'UTR. The ER marker, PfSec12 was expressed as an mRFP-fusion from the plasmid pML2 (S*19*).

Parasite transfection was performed as previously described (S*20*). The $Dd2^{attB}$ parasite line was continuously cultured in the presence of 2.5 nM WR99210 (Jacobus Pharmaceuticals, Princeton, NJ), and upon cotransfection with both the pDC2-attP expression plasmid and the integrase-containing plasmid pINT, was additionally treated with 2 µg/ml Blasticidin S (Invitrogen) and 125 µg/ml G418 sulfate (Cellgro). Integration was confirmed by PCR amplification of the attB-attP recombinant locus (Fig. S4C). For cotransfection of the PfATP4-GFP and mRFP-PfSec12 expression plasmids, Dd2 parasites were selected with 2 µg/ml Blasticidin S and 2.5 nM WR99210 the day after transfection.

Fluorescent parasites were examined using a Nikon Ti-E inverted microscope (Melville, NY) with 100 $\times$ N. A. 1.4 PlanApo optics and a CoolSnap HQ2 camera. Images were

collected with Nikon NIS Elements software and assembled using Adobe Photoshop (Adobe Systems, Mountain View, CA).

Homology modeling

Homology modeling was performed by using DeepView/Swiss pdb viewer v.4.0.1 (http://www.expasy.org/spdbv/) and SWISS-MODEL (Automated Protein Modelling Server) (S*21*). PfATP4 amino acid residues 118–1261 were aligned to the crystal structure of the calcium-free E2 state of the rabbit sarcoplasmic reticulum Ca^{2+} -ATPase, stabilized by the inhibitor thapsigargin and the nonhydrolyzable ATP analog AMPPCP (Protein Data Bank accession number 2C88) (S*22*). The geometry of the model was refined in REFMAC5 located in the CCP4 Program Suite version 6.0.0 (Collaborative Computational Project No. 4, Warrington, UK). PyMol (The PyMOL Molecular Graphics System, Version 1.2, Schrödinger, LLC) was used to visualize the model and generate figures.

Xenopus laevis oocyte expression studies and ATP hydrolysis measurements

Vector construction and *Xenopus* oocyte expression was completed following the general strategies employed by Krishna et al. (S*23*). In brief, PCR-amplification of sequence-verified *pfatp4* genes was accomplished using the following primers: ATATCTAGA**CCACC**ATGAGTTCTCAA (strong Kozak sequence in bold, *Xba*I site underlined) and ATAGAGCTC**TTA**ATTCTTAATAGTCATATATTTTCTTC (stop codon in bold, *Sac*I site underlined). Restriction digested PCR products were ligated into the *Xba*I/*Xho*I sites in pSP64 and positive clones were validated by DNA sequencing. *In vitro* transcribed capped cRNA was made using the mMESSAGE mMACHINE^{TM} SP6 kit (Ambion, Austin, TX, USA) from *EcoR*I-linearized template. An extended polyA tail was added using the Poly(A) Tailing Kit (Ambion, Austin, TX, USA). SUPERase-In (1 U/µL) was added to protect the capped cRNA from degradation and stored at -20°C.

Xenopus oocytes were harvested, connective tissue removed and stages V and VI oocytes were selected. Oocytes were microinjected with cRNA (5–30 ng) encoding alleles of *pfatp4* from either wild-type, NITD609-R^{Dd2} clone #1, NITD609-R^{Dd2} clone #3 or RNase-free water (50 nl). Oocytes were subsequently incubated (at 19°C) in Barth's solution for 3 days.

Total membrane preparations from oocytes were obtained by homogenizing 30-35 oocytes in ~800µL oocyte lysis buffer (83mM NaCl, 1mM $MgCl_2$, and 50mM Tris, pH 7.4 supplemented with a Roche EDTA-free Complete protease inhibitor cocktail tablet). Oocyte homogenates were centrifuged at 1000 ×g for 5 min and the supernatant was removed. The remaining pellet was resuspended in a second volume of lysis buffer and recentrifuged. The supernatants were pooled and subjected to ultracentrifugation on a Beckman Optima LE-80k (SW60-Ti rotor; 100,000 × g, 90 min) to pellet the membrane fraction. The pellets were stored at -80°C.

Ca^{2+}-ATPase activity was monitored by a coupled enzyme assay described by Krishna et al. (S*23*). Briefly, membranes (5 µg of protein) were mixed in a volume of 50 µl containing ATP (2 mM), phospho(enol)pyruvate (2.5 mM), NADH (0.25 mM), pyruvate kinase (7.5 units), and lactate dehydrogenase (8.0 units). The oxidation rate of NADH was recorded at A_{340} (Shimadzu UV-800; Shimadzu Corporation, Kyoto, Japan) in the absence and presence of 25µM $[Ca^{2+}]_{free}$.

References

S1. Y. Y. Lau, E. Sapidou, X. Cui, R. E. White, K. C. Cheng, *Drug Metab Dispos* **30**, 1446 (Dec, 2002).
S2. W. Trager, J. B. Jensen, *Science* **193**, 673 (1976).
S3. R. E. Desjardins, C. J. Canfield, J. D. Haynes, J. D. Chulay, *Antimicrobial agents and chemotherapy* **16**, 710 (Dec, 1979).
S4. C. Lambros, J. P. Vanderberg, *J Parasitol* **65**, 418 (Jun, 1979).
S5. S. Maerki, R. Brun, S. A. Charman, A. Dorn, H. Matile, S. Wittlin, *J Antimicrob Chemother* **58**, 52 (Jul, 2006).
S6. B. Franke-Fayard, H. Trueman, J. Ramesar, J. Mendoza, M. van der Keur, R. van der Linden, R. E. Sinden, A. P. Waters, C. J. Janse, *Mol Biochem Parasitol* **137**, 23 (Sep, 2004).
S7. K. Sriprawat, S. Kaewpongsri, R. Suwanarusk, M. L. Leimanis, U. Lek-Uthai, A. P. Phyo, G. Snounou, B. Russell, L. Renia, F. Nosten, *Malar J* **8**, 115 (2009).
S8. B. Russell, F. Chalfein, B. Prasetyorini, E. Kenangalem, K. Piera, R. Suwanarusk, A. Brockman, P. Prayoga, P. Sugiarto, Q. Cheng, E. Tjitra, N. M. Anstey, R. N. Price, *Antimicrobial agents and chemotherapy* **52**, 1040 (Mar, 2008).
S9. B. M. Russell, R. Udomsangpetch, K. H. Rieckmann, B. M. Kotecka, R. E. Coleman, J. Sattabongkot, *Antimicrobial agents and chemotherapy* **47**, 170 (Jan, 2003).
S10. W. W. Sharrock, R. Suwanarusk, U. Lek-Uthai, M. D. Edstein, V. Kosaisavee, T. Travers, A. Jaidee, K. Sriprawat, R. N. Price, F. Nosten, B. Russell, *Malar J* **7**, 94 (2008).
S11. D. Plouffe, A. Brinker, C. McNamara, K. Henson, N. Kato, K. Kuhen, A. Nagle, F. Adrian, J. T. Matzen, P. Anderson, T. G. Nam, N. S. Gray, A. Chatterjee, J. Janes, S. F. Yan, R. Trager, J. S. Caldwell, P. G. Schultz, Y. Zhou, E. A. Winzeler, *Proc Natl Acad Sci U S A* **105**, 9059 (Jul 1, 2008).
S12. R. S. Obach, *Drug Metab Dispos* **27**, 1350 (Nov, 1999).
S13. R. S. Obach, J. G. Baxter, T. E. Liston, B. M. Silber, B. C. Jones, F. MacIntyre, D. J. Rance, P. Wastall, *J Pharmacol Exp Ther* **283**, 46 (Oct, 1997).
S14. M. Traebert, B. Dumotier, L. Meister, P. Hoffmann, M. Dominguez-Estevez, W. Suter, *Eur J Pharmacol* **484**, 41 (Jan 19, 2004).
S15. M. S. Diehl, S. L. Willaby, R. D. Snyder, *Environ Mol Mutagen* **36**, 72 (2000).
S16. N. V. Dharia, A. B. Sidhu, M. B. Cassera, S. J. Westenberger, S. E. Bopp, R. T. Eastman, D. Plouffe, S. Batalov, D. J. Park, S. K. Volkman, D. F. Wirth, Y. Zhou, D. A. Fidock, E. A. Winzeler, *Genome Biol* **10**, R21 (Feb 13, 2009).
S17. C. Kidgell, S. K. Volkman, J. Daily, J. O. Borevitz, D. Plouffe, Y. Zhou, J. R. Johnson, K. Le Roch, O. Sarr, O. Ndir, S. Mboup, S. Batalov, D. F. Wirth, E. A. Winzeler, *PLoS pathogens* **2**, e57 (Jun, 2006).
S18. L. J. Nkrumah, R. A. Muhle, P. A. Moura, P. Ghosh, G. F. Hatfull, W. R. Jacobs, Jr., D. A. Fidock, *Nat Methods* **3**, 615 (Aug, 2006).
S19. M. C. Lee, P. A. Moura, E. A. Miller, D. A. Fidock, *Mol Microbiol* **68**, 1535 (Jun, 2008).
S20. D. A. Fidock, T. E. Wellems, *Proc Natl Acad Sci U S A* **94**, 10931 (Sep 30, 1997).
S21. K. Arnold, L. Bordoli, J. Kopp, T. Schwede, *Bioinformatics* **22**, 195 (Jan 15, 2006).
S22. A. M. Jensen, T. L. Sorensen, C. Olesen, J. V. Moller, P. Nissen, *EMBO J* **25**, 2305 (Jun 7, 2006).
S23. S. Krishna, C. Woodrow, R. Webb, J. Penny, K. Takeyasu, M. Kimura, J. M. East, *J Biol Chem* **276**, 10782 (Apr 6, 2001).